# Ym1 protein crystals promote type 2 immunity

**Ines Heyndrickx[1,2], Kim Deswarte[1,2], Kenneth Verstraete[3,4], Koen H. G. Verschueren[3,4], Ursula Smole[1,2], Helena Aegerter[1,2], Ann Dansercoer[3,4], Hamida Hammad[1,2], Savvas N. Savvides[3,4], Bart N. Lambrecht[1,2,5]**

[1]Laboratory of Immunoregulation and Mucosal Immunology, VIB-UGent Center for Inflammation Research, Ghent, Belgium.
[2]Department of Internal Medicine and Pediatrics, Ghent University, Ghent, Belgium.
[3]Unit for Structural Biology, VIB-UGent Center for Inflammation Research, Ghent, Belgium.
[4]Department of Biochemistry and Microbiology, Ghent University, Ghent, Belgium.
[5]Department of Pulmonary Medicine, Erasmus University Medical Center Rotterdam, Rotterdam, The Netherlands.

**Abstract (165 words)**

*Background:* Spontaneous protein crystallization is a rare event, yet needle-shaped protein crystals are frequently found in eosinophil-rich inflammation. In humans, Charcot-Leyden crystals (CLCs) are made from galectin-10 (Gal10) protein, an abundant protein in eosinophils.
*Aim:* Whereas mice do not encode Gal10 in their genome, they do form pseudo-CLCs, made from the chitinase-like proteins Ym1 and/or Ym2, encoded by *Chil3* and *Chil4* and made by myeloid and epithelial cells respectively. Here, we investigated the biological effects of pseudo-CLCs since their function is currently unknown.
*Methods and results:* We produced recombinant Ym1 crystals which were shown to have identical crystal packing and structure by X-ray crystallography as *in vivo* native crystals derived from murine lung. When administered to the airways of mice, crystalline but not soluble Ym1 stimulated innate and adaptive immunity and acted as a type 2 immune adjuvant for eosinophilic inflammation via triggering of dendritic cells (DCs).
*Conclusion:* Murine Ym1 protein crystals found at sites of eosinophilic inflammation reinforce type 2 immunity and could serve as a surrogate model for studying the biology of human CLCs.

**Corresponding author** Bart N. Lambrecht, MD, PhD
Bart.Lambrecht@ugent.be

**Keywords:** adjuvanticity, protein crystals, Ym1, Ym2, Charcot-Leyden Crystals, Chitinase-like proteins

**Running Title**: *Pseudo-Charcot Leyden Crystals*

**eBlurb:** Protein crystallization is exceedingly rare, yet here, Heyndrickx et al. show that Ym1 crystals made from the chitinase like protein Chil3 promote type 2 immunity in mice.

**Acknowledgements and Funding**

We acknowledge the crucial help of the staff of the VIB Bioimaging core, the VIB Flow Cytometry core and the VIB Protein Synthesis Core. B.N.L. acknowledges support from ERC advanced grant (789384 ASTHMA CRYSTAL CLEAR), a concerted research initiative grant from Ghent University (GOA, 01G010C9), an FWO Methusalem grant (01M01521) and an FWO EOS research grant (3G0H1222), and the Flanders Institute of Biotechnology (VIB). S.N.S. acknowledges support to this project from the Ghent University GOA program (grant no. BOF17-GOA-028),. S.N.S, K.V., and K.H.G.V. thank the staff and management of synchrotron beamlines P14 (PETRA 3, Hamburg, Germany), Proxima 1 (SOLEIL, Saclay, France), and PX1 (Swiss Light Source, Villigen, Switzerland) for beamtime allocation and support during data collection of X-ray diffraction data.

## Introduction

Protein crystals have been described already 150 years ago in eosinophilic inflammatory lesions in humans by Charcot and von Leyden [1-3]. Most proteins can only function properly in the soluble state and spontaneous protein crystallization *in vivo* remains a rare and largely unsolved scientific enigma [4,5].

Protein crystals have also been documented in mouse tissues, almost exclusively in the context of type 2 inflammation, rich in eosinophils, Th2 cells and alternatively activated macrophages [6-22]. Unstained crystals are colorless, but in histochemical stains they stain brightly with eosin, consistent with their protein content [14]. Before their biochemical nature was elucidated, they were therefore often referred to as eosinophilic crystals [6]. These murine crystals are frequently observed in aged mice and genetically altered mice on a C57BL/6 or Sv/129 background, and in the context of eosinophil-rich asthma and parasitic infections [6,23]. Although eosinophilic crystals have been documented in the skin, biliary tree, stomach, lymph nodes, spleen and bone marrow of mice, it is clear that the principal site of crystal accumulation is in the lung. In several descriptions, accumulation of eosinophilic crystals was associated with severe lung inflammation and the disease was called eosinophilic crystalline pneumonia, acidophilic macrophage pneumonia or crystalline pneumonitis [7,17,23,24]. The accumulated crystals are variable in size and shape ranging from needle-like crystals to rectangular plates [14]. Their resemblance to the needle-shaped human Charcot-Leyden crystals (CLCs) frequently resulted in the incorrect identification of these murine crystals as CLCs [24,25]. However, only in 2000, almost 100 years after they were first described, Guo *et al*. purified crystals from the bronchoalveolar lavage (BAL) fluid of viable motheaten ($me^v/me^v$) mice and mass spectrometry analysis identified the chitinase-like protein (CLP) Ym1 as the sole protein component [6], thereby providing an unambiguous annotation of their content and distinguishing them from CLCs. Human CLCs are comprised of the eosinophil-derived galectin-10 (Gal10) protein, which is not encoded in the mouse genome [26,27]. Ym1 is produced by a subset of circulating pro-repair monocytes, by alternatively activated "M2" macrophages, alveolar macrophages, and by neutrophils [28-30]. In hyaline gastric lesions of aged 129S4/SvJae and B6,129 CYP1A2 null mice, pseudo-CLCs were found to consist of the closely related CLP Ym2, which is a protein mainly made by epithelial cells under the influence of IL-13 [14,25,31,32]. Ym1 (encoded by the *Chil3* gene) and Ym2 (encoded by the *Chil4* gene) are CLPs belonging to the glycoside hydrolase family 18 (GH18) and are unique to mice, with no known human orthologues [33]. Their potential receptors and natural binding partners are largely unknown, as are the exact functions of these still very enigmatic proteins.

We previously reported that recombinant Gal10 crystals produced *in vitro* showed crystal packing and structure identical to CLCs derived from patient mucus. When administered to the airways of mice, Gal10 crystals stimulated innate and adaptive immunity and acted as a type 2 adjuvant [34]. Since mice do not encode the *LGALS10* gene, Gal10 has the potential to act as a neo-antigen in this setting. Here, we tested the *in vivo* relevance of pseudo-CLCs since these are made endogenously in mice at sites of eosinophilic inflammation, albeit by macrophages and epithelial cells. Furthermore, given the high sequence identity of Ym1 and

Ym2 we hypothesized whether Ym2 might also crystallize *in vivo* analogous to Ym1. Recombinant *in vitro* made Ym1 and Ym2 crystals were biosimilar to crystals isolated from mice, and when administered to the airways of mice, crystalline Ym1, but not soluble Ym1 protein stimulated innate and adaptive immunity and acted as an adjuvant for Th2 driven eosinophilic airway inflammation and immunoglobulin secretion.

100 **Methods**

101 **Mice**

102 Female wild type (WT) C57BL/6 mice were purchased from Janvier Labs (Saint-Berthevin,
103 France), housed under specific pathogen-free conditions and used between 6 and 8 weeks of
104 age. Investigators were not blinded to group allocation during experiments. No animals were
105 excluded from the analysis. All experiments were approved by the animal ethics committee at
106 Ghent University and were in accordance with Belgian animal protection law.

107

108 **Production of recombinant Ym1 and Ym2 protein and crystals**

109 A synthetic codon-optimized DNA sequence (Genscript) encoding murine Ym1 (Uniprot ID
110 O35744, residues 22 – 398) was cloned in the pCAGG mammalian expression vector in frame
111 with the mouse IgH signal peptide (MGWSCIIFFLVATATGVHS). A synthetic codon-optimized
112 DNA sequence (Genscript) encoding murine Ym2 (Uniprot Q91Z98, residues 22 - 402) was
113 cloned in the pTwist-CMV-BetaGlobin mammalian expression vector (Twist Biosciences), in
114 frame with the mouse IgH signal peptide (MGWSCIIFFLVATATGVHS), and an N-terminal
115 hexahistine-tag followed by a Tobacco Etch Virus (TEV)-protease cleavage site.

116 Ym1 and Ym2 were produced in FreeStyle 293-F cells in suspension. Cells were transfected
117 with 1 μg/ml DNA using 2-fold excess of linear polyethylenimine (PEI; Polysciences).
118 Conditioned medium containing the secreted recombinant protein was collected 4 days post
119 transfection, filtered and dialyzed to 20 mM Tris pH 8.0. Ym1 was purified via Q Sepharose
120 anion exchange chromatography. Ym1 was further purified to a pure solution via size-
121 exclusion chromatography, while Ym2 was purified from the clarified conditioned medium via
122 immobilized metal affinity chromatography (IMAC) and size-exclusion chromatography with
123 phosphate-buffered saline (PBS) buffer. Endotoxin levels were determined with an Endosafe-
124 PTS system (Charles River) to be lower than 1 EU/mg of recombinant protein. To form
125 recombinant Ym1 crystals, recombinant Ym1 protein (3 to 4 mg/ml) was incubated with 1M
126 Na-acetate buffer pH 4.6 with a buffer:target protein ratio of 1:10 (v/v). During a 24h
127 incubation the protein solution was agitated a few times by inverting it five times, after which
128 the solution turned cloudy due to the formation of protein crystals. The crystal-containing
129 suspension was spun down (400g for 5 min) and washed three times with sterile and
130 endotoxin-free PBS before the crystals were resuspended in 1 ml of sterile and endotoxin-free
131 PBS. The total protein concentration of this solution was determined by solubilizing 20 µl of
132 the crystal suspension in an equal volume of 6M guanidinium hydrochloride and measuring
133 the absorbance at 280 nm with a Thermo Scientific NanoDrop 2000. The calculated extinction
134 coefficient for Ym1 was 77155 $M^{-1}$ $cm^{-1}$.

135

136 **Crystallographic structure determination of *ex vivo* and recombinant Ym1 and Ym2 crystals**

137 Single *ex vivo* Ym1 and Ym2 crystals were harvested from the BAL fluid of $me^v/me^v$ mice and
138 C57BL/6J-Tg(CAG-Gal10)Bla mice by using mounted cryo-loops. Before being cryo-cooled in
139 liquid nitrogen, crystals were cryo-protected by a brief soak in PBS supplemented with 35%
140 (v/v) ethylene glycol (Ym1) or 35 % glycerol (Ym2). Recombinant Ym1 was crystallized in

141 condition A7 of the Hampton Research Crystal Screen HT (0.1 M sodium cacodylate pH 6.5,
142 1.4 M sodium acetate) via vapor diffusion sitting drop crystallization experiments, and crystals
143 were cryo-protected with mother liquor supplemented with 30% (v/v) glycerol. Following
144 overnight incubation with TEV-protease, recombinant Ym2 was crystallized via vapor diffusion
145 sitting drop crystallization experiments using 0.1 M sodium acetate pH 6.0 and 200 mM $CaCl_2$
146 as mother liquor, and crystals were cryoprotected with 30% (v/v) PEG-400. Diffraction
147 experiments at 100 K were conducted on beamlines Proxima 1 (SOLEIL synchrotron, Saint-
148 Aubin, France), P14 of Petra III (DESY, Hamburg, Germany) and X06SA (PXI) of the Swiss Light
149 Source (Paul Scherrer Institute, Villigen, Switzerland). All data were integrated and scaled
150 using the XDS suite[35] and the CCP4 suite [36]. Molecular replacement was executed using Phaser
151 [37] employing the structure of Ym1 (pdb: 1vfb) as a search model. Further rebuilding of the
152 model and refinement was performed in *COOT* [38] and autoBuster [39]. Map and model validation
153 was monitored throughout the refinement procedure using *COOT*, the CCP4 package and
154 PDB_REDO server [40].
155
156 ***In vivo* models**
157 To analyze the innate immune responses, WT C57BL/6 mice were injected intratracheally (i.t.)
158 with 100 µg Ym1 crystals or 100 µg soluble Ym1 diluted in 80 µl of PBS. After 6 and 24 hours,
159 mice were euthanized by $CO_2$ inhalation or an overdose of pentobarbital (KELA Laboratoria)
160 and BAL fluid and lungs were collected.
161 To analyze dendritic cell (DC) activation, WT C57BL/6 mice were injected i.t. with 5 µg Alexa
162 Fluor 488-labeled ovalbumin (OVA-AF488) mixed with 100 µg Ym1 crystals or with 100 µg
163 soluble Ym1 diluted in 80 µl of PBS. After 24 hours, mice were euthanized by $CO_2$ inhalation
164 and mediastinal lymph nodes (mLNs) were collected.
165 To analyze the adaptive cellular immune responses, CD4+ OT-II KN2 cells were purified from
166 CD45.1.2 OT-II KN2 donor mice with the MojoSort™ Mouse CD4 T Cell Isolation Kit (Biolegend)
167 and labeled with cell proliferation dye eFluor 450 (0.01 mM; Thermo Fisher Scientific) for 10
168 min in the dark at 37°C. Next, $1 \times 10^6$ of these labeled cells (in 100 µl of PBS) were injected
169 intravenously (i.v.) into WT C57BL/6 mice and subsequentelly, mice were injected i.t. with 10
170 µg ovalbumin (OVA, Worthington) or with 10 µg OVA mixed with 100 µg of Ym1 crystals or
171 100 µg soluble Ym1 (in 80 µl of PBS). For this experiment, OVA was pre-filtered through a 0.22
172 µm filter. On day 4 and 7, mice were euthanized by $CO_2$ inhalation and mLNs and lungs were
173 collected.
174 To analyze the adaptive humoral immune responses, WT C57BL/6 mice were injected
175 intraperitoneally (i.p.) on day 0 with 0.5 mg Ym1 crystals or 0.5 mg soluble Ym1, on day 7 with
176 0.5 mg Ym1 crystals and on day 14 with 0.5 mg Ym1 crystals or 10 µg Sol Ym1 all diluted in 500
177 µl PBS. On day 21 mice were euthanized with an overdose of pentobarbital (KELA Laboratoria)
178 and blood was collected.
179 To analyze the type 2 adjuvanticity of Ym1 crystals, WT C57BL/6 mice were sensitized i.t. on
180 day 0 and day 1 with 100 µg OVA (Worthington), 100 µg OVA mixed with 100 µg of Ym1 crystals
181 or 100 µg OVA mixed with 100 µg soluble Ym1 diluted in 80 µl PBS. On days 11 to 13, all mice

were challenged daily intranasally (i.n.) with 20 µg of OVA (Worthington) diluted in 40 µl of PBS. One day after the last challenge, on day 14, mice were euthanized with an overdose of pentobarbital (KELA Laboratoria) and blood, BAL fluid and mLNs were collected.

All i.t. and i.n. treatments were given after mice were anesthetized with isoflurane (2 liters/min, 2 to 3%; Abbott Laboratories).

Blood was obtained from the iliac vein and centrifuged at 10000 rpm for 10 min at room temperature (RT). Serum was collected and stored at −20 °C until further use (serum antibody ELISA). BAL was performed by injecting PBS containing 0.01 mM EDTA (Lonza) through a tracheal canula. Subsequently, BAL fluid was centrifuged (400g for 5 min at 4°C). The supernatant was collected and stored at −20°C until further use (cytokine ELISA) and the pellet was used for ImageStream or flow cytometry. To obtain lung and mLN single-cell suspensions for flow cytometry, lungs and mLNs were first cut with a scissor and then digested at 37°C for 30 or 15 min respectively in RPMI-1640 (ThermoFisher Scientific) containing Liberase TM (20 µg/ml; Merck) and deoxyribonuclease (DNase) I (0.01 U/µl; Merck). The resultant cell suspensions were filtered through a 70 µm filter. To obtain mLN single-cell suspensions for flow cytometry or mLN restimulation cultures, mLNs were smashed on a 70 µm filter. To measure pro-inflammatory cytokines, lungs were snap frozen in liquid nitrogen and homogenized with a TissueLyser II from Qiagen in tissue lysis buffer [40 mM tris-HCL (pH 6.8), 275mM NaCl and 20% glycerol (Sigma-Aldrich)]. One tablet of PhosSTOP (Sigma-Aldrich) and one tablet of Complete ULTRA tablets, Mini, Easypack (Sigma-Aldrich) were added per 10 ml of tissue lysis buffer. After homogenization, 2% IGEPAL CA-630 (U.S. Biological) was added. Subsequently, the samples were rotated for 30 min and centrifuged (20000g for 10 min at 4°C). Supernatants were stored at −20°C. The total protein concentration was measured with the NanoOrange protein quantitation kit from Thermo Fisher Scientific.

**Flow cytometry**

Prior to staining for flow cytometry, single-cell suspensions were depleted of red blood cells (RBCs) by using RBC lysis buffer [0.15 M NH4Cl (Merck), 1 mM KHCO3 (Merck), and 0.1 mM Na2-EDTA (Merck) in MilliQ H2O] produced in-house. For all flow experiments, single cell suspensions were incubated with the eBioscience™ Fixable Viability Dye eFluor™ 506 (ThermoFisher Scientific) to identify dead cells. Fc Block 2.4.G2 (Bioceros) was used to block aspecific antibody binding. Cell surface markers were stained for 30 min at 4°C in the dark. 123count eBeads™ Counting Beads (ThermoFisher Scientific) were added to each sample to determine absolute cell numbers. Settings were calibrated using UltraComp eBead™ Compensation Beads (ThermoFisher Scientific). Data were acquired on an LSR Fortessa with FACS Diva software (BD Biosciences) and were analyzed with FlowJo software (Tree Star).

For the analysis of innate immune responses, lung single-cell suspensions were stained for flow cytometry using FITC-conjugated anti-Ly-6C (AL-21) (BD Biosciences), PE-conjugated anti-Siglec-F (E50-2440) (BD Biosciences), PE-Cy5-conjugated anti-CD3e (145-2c11) (Thermo Fisher Scientific), PE-Cy5-conjugated anti-CD19 (1D3) (Thermo Fisher Scientific), PE-Cy7-conjugated anti-CD11c (N418) (Thermo Fisher Scientific), BD Horizon V450-conjugated anti-CD11b

223 (M1/70) (BD Biosciences), Brilliant Violet 605-conjugated anti-CD45 (30-F11) (BD Biosciences),
224 Alexa Fluor 647-conjugated anti-CD64 (X54-5/7.1) (BD Biosciences), Alexa Fluor 700–
225 conjugated anti-Ly6G (1A8) (BD Biosciences) and APC-eFluor 780–conjugated anti-I-A/I-E
226 (M5/114.15.2) (Thermo Fisher Scientific).
227 For the analysis of DC activation, mLN single-cell suspensions were stained for flow cytometry
228 using PerCP-Cy5.5-conjugated anti-CD80 (16-10A1) (BioLegend), eFluor 450-conjugated anti-
229 CD11c (N418) (ThermoFisher Scientific), Brilliant Violet 650-conjugated anti-XCR1 (ZET)
230 (BioLegend), Brilliant Violet 711-conjugated anti-CD64 (X54-5/7.1) (BioLegend), Alexa Fluor
231 647-conjugated anti-CD172a (P84) (BioLegend), Alexa Fluor 700- conjugated anti-Ly-6C (AL-
232 21) (BD Biosciences), APC-eFluor 780-conjugated anti-MHCII (M5/114.15.2) (ThermoFisher
233 Scientific), PE-conjugated anti-CD88 (20/70) (BioLegend), biotin-conjugated anti-CCR7 (4B12)
234 (ThermoFisher Scientific) + PE-CF594-conjugated streptavidin (BD Biosciences), PE-Cy5-
235 conjugated anti-CD3e (145-2c11) (ThermoFisher Scientific), PE-Cy5-conjugated anti-CD19
236 (1D3) (Thermo Fisher Scientific), PE-Cy7-conjugated anti-CD86 (PO3) (BioLegend), BUV395-
237 conjugated anti-CD11b (M1/70) (BD Biosciences) and BUV737-conjugated anti-CD26 (H194-
238 112) (BD Biosciences).
239 For T cell response analysis, mLN and lung single-cell suspensions were stained using
240 FITC-conjugated anti-Va2 TCR (B20.1) (BD Biosciences), Brilliant Violet 605-conjugated anti-
241 CD45.1 (A20) (BioLegend), RedFluor710-conjugated anti-CD44 (IM7) (Thermo Fisher
242 Scientific), APC-eFluor780-conjugated anti-CD25 (PC61.5) (Thermo Fisher Scientific), PE-
243 conjugated anti-CD62L (MEL-14) (BD Biosciences), biotin-conjugated anti-hCD2 (RPA-2.10)
244 (BioLegend) + PE-CF594-conjugated streptavidin (BD Biosciences), PE-Cy7-conjugated CD3e
245 (145-2C11) (BioLegend), BUV395-conjugated anti-CD4 (GK1.5) (BD Biosciences) and BUV737-
246 conjugated anti-CD45.2 (104) (BD Biosciences).
247 BAL cells were stained with PE-conjugated anti-Siglec F (E50-2440) (BD Biosciences), PE-Cy5-
248 conjugated anti-CD3e (145-2c11) (ThermoFisher Scientific), PE-Cy5-conjugated anti-CD19
249 (1D3) (Thermo Fisher Scientific), PE-Cy7-conjugated anti-CD11c (N418) (ThermoFisher
250 Scientific), BD Horizon V450-conjugated anti-CD11b (M1/70) (BD Biosciences), Alexa Fluor
251 700-conjugated anti-Ly6G (1A8) (BD Biosciences) and APC-eFluor 780-conjugated anti-MHCII
252 (M5/114.15.2) (Thermo Fisher Scientific).
253
254 **ImageStream**
255 For ImageStream analysis, the pellets obtained after centrifugation of the BAL fluid were
256 pooled and stained for 30 min at 4°C with unconjugated polyclonal goat anti-mouse Ym1/2
257 (AF2446, R&D Systems; 1:100 diluted in PBS). After washing, the pellet was stained for 30 min
258 at 4°C in the dark with Alexa Fluor 647-conjugated polyclonal donkey anti-goat IgG
259 (ThermoFisher Scientific; 1:1000 diluted in PBS). Fc Block 2.4.G2 (Bioceros) was used to block
260 aspecific antibody binding. Data were acquired on an Amnis ImageStreamX Mk II with
261 INSPIRE™ software (Luminex) and were analyzed with IDEAS® software (Luminex).
262
263 **Enzyme-linked immunosorbent assay (ELISA)**

264 Interleukin (IL)-1β, IL-5, IL-6, IL-10, IL-13, IL-33, tumor necrosis factor alpha (TNFα) and C-C
265 motif chemokine ligand 2 (CCL2) concentrations were evaluated using the Ready-SET-Go!™
266 ELISA kits (ThermoFisher Scientific). CCL24 concentrations were evaluated using the Mouse
267 CCL24/Eotaxin-2/MPIF-2 DuoSet ELISA kit (R&D Systems). Serum Ym1-specific
268 immunoglobulin M (IgM) and OVA-specific immunoglobulin G1 (IgG1) antibody levels were
269 determined in flat-bottom 96-well plates (Greiner Bio-One), coated overnight with 0.1 mg/ml
270 soluble Ym1 in PBS or with 0.1 mg/ml OVA (Worthington) in 0.1 M sodium carbonate buffer
271 (pH 9.5), respectively. After washing and blocking for 1 hour, the samples diluted in PBS were
272 added in duplicate and incubated for 2.5 hours at RT. After washing, biotinylated anti-mouse
273 IgG1 or IgM detecting antibody (0.5 mg/ml; BD Biosciences) plus streptavidin-HRP reagent
274 (1:250; BD Biosciences) was added and incubated for 1 hour at RT. After another wash step,
275 1× TMB substrate solution (Thermo Fisher Scientific) was added and to stop the reaction, 2.5N
276 $H_2SO_4$ was used. Finally, the absorbance was read at 450 nm (and 650 nm as reference) with
277 a Perkin Elmer multilabel counter and data were collected with Wallac 1420 Manager software
278 (PerkinElmer).
279
280 **Statistical analysis**
281 Experiments shown in Figure 2 were analyzed with an ordinary two-way ANOVA test with
282 Tukey's multiple comparisons test. For all experiments in Figure 3, 4 and 5, the normality of
283 each group was first checked by using the Shapiro-Wilk statistical test. Parametric data were
284 analyzed with an ordinary one-way ANOVA test with Šidák's multiple comparison correction
285 and nonparametric data were analyzed with a Kruskal-Wallis test with Dunn's multiple
286 comparison correction. All statistical tests were performed in GraphPad Prism software
287 (GraphPad Software).
288
289 **Supplementary Online Material**
290 This paper has an online data supplement. Table S1 describes the key crystallographic data of
291 ex vivo isolated Ym1 and Ym2 crystals for comparison with in vitro generated recombinant
292 Ym1 and Ym2 crystals.

293 **Results**

294 **Recombinant Ym1 and Ym2 crystals are structurally similar to native crystals *ex vivo*.**

295 Individual crystals were harvested from the BAL fluid of $me^v/me^v$ mice (carrying a defective
296 protein tyrosine phosphatase SHP-1 gene) developing crystalline pneumonia [6] and C57BL/6J-
297 Tg (*Cagg-Gal10*)$^{Bla}$ mice (transgenically overexpressing Gal10 from the ubiquitous *Cagg*
298 promotor, manuscript in preparation), sensitized and challenged with the allergen house dust
299 mite (HDM). Crystallographic studies using microfocus synchrotron X-rays showed that the
300 crystals obtained from the BAL fluid of $me^v/me^v$ mice were Ym1 crystals, in accordance with a
301 previous report [6]. We had hypothesized that the crystals obtained from the BAL fluid of
302 C57BL/6J-Tg(CAG-Gal10)Bla mice were CLCs containing Gal10. However, crystallographic
303 characterization of these crystals revealed that they are Ym2 crystals. In parallel, we produced
304 recombinant Ym1 and Ym2 protein in FreeStyle 293-F cells. Spontaneous crystallization was
305 aided by low pH and low temperature (4°C) (Fig. 1 A, B). Native *in vivo* isolated Ym1 crystals
306 and recombinant Ym1 crystals (Fig. 1 C) as well as native *in vivo* isolated Ym2 crystals and
307 recombinant Ym2 crystals (Fig. 1 D) were crystallographically equivalent, sharing the same
308 hexagonal space group (P21) and unit-cell parameters. Moreover, X-ray crystallographic
309 studies showed that a native *in vivo* isolated Ym1 crystal and a native *in vivo* isolated Ym2
310 crystal are structurally similar to each other, which is not so surprisingly as Ym1 (*Chil3*) and
311 Ym2 (*Chil4*) are two closely related proteins sharing 95% nucleotide sequence identity and
312 91% amino acid sequence identity (Fig. 1 E, F, G). Crystallographic data and refinement
313 statistics can be found in Table S1. Thus, recombinant Ym1 and Ym2 protein crystals can be
314 generated *in vitro* and are biosimilar to native Ym1 and Ym2 crystals.

315

316 **Ym1 crystals activate innate immunity.**

317 We next addressed whether Ym1 crystals could have pro-inflammatory effects in the lungs.
318 Naïve WT C57BL/6 mice received an i.t. injection of 100 µg of endotoxin-low Ym1 crystals or
319 control soluble Ym1 (Fig. 2 A). After 6 and 24 hours, there was a prominent influx of $Ly6C^+$
320 monocytes and eosinophils into the airways of mice receiving Ym1 crystals but not in those
321 receiving soluble Ym1 or PBS. Neutrophil numbers were also increased in the Ym1 crystal
322 group, but this failed to reach statistical significance (Fig. 2 B). This influx was accompanied by
323 the production of the innate pro-inflammatory cytokines IL-6 and TNFα in BAL fluid (Fig. 2 C)
324 and the inflammasome-dependent cytokine IL-1β and the alarmin IL-33 in lung tissue only in
325 the group receiving crystalline Ym1 (Fig. 2D). Other cytokines like IL-1α and GM-CSF were not
326 consistently induced in any of the groups (data not shown). The monocyte chemoattractant
327 CCL2 and the eosinophil chemoattractant CCL24 (Eotaxin-2) were found enhanced in lung
328 tissue of the crystal-treated group (Fig. 2 E), particularly at early time points, suggesting these
329 paracrine signals were driving the cellular influx induced by crystals. Cellular influx and
330 production of these cytokines and chemokines was also observed in earlier work where
331 recombinant Gal10 crystals or uric acid (UA) crystals were injected into the lungs of mice,
332 suggesting this is a generic response to crystals of different chemical composition[34,41].

333 As we were unable to make a crystallization-deficient soluble Ym1 mutein, we used WT soluble
334 Ym1 protein as a control. However, we took into consideration that soluble Ym1 might
335 crystallize *in vivo* after i.t. injection. To test this, we stained BAL pellets using a polyclonal anti
336 Ym1/2 antibody and analyzed the samples using the ImageStream flow cytometry platform.
337 The results clearly showed that the i.t. injected pre-formed Ym1 crystals were still present as
338 intact crystals after 6 and 24 hours. The soluble Ym1 protein indeed crystallized *in vivo,* with
339 crystals being clearly detectable after 6 hours and accumulating further after 24 hours. The
340 crystals formed *in vivo* after i.t. injection of soluble Ym1 were also plate-like, but had a less
341 uniform distribution and were smaller in size than the i.t. injected Ym1 crystals (Fig. 2 F). The
342 total number of crystals found in the BAL pellet of soluble Ym1 treated mice (266 crystals in 5
343 pooled BAL pellets) was lower than in the BAL pellet of Ym1 crystal treated mice (1355 crystals
344 in 5 pooled BAL pellets), potentially explaining why the soluble Ym1 group had less
345 inflammation compared with the group receiving pre-formed Ym1 crystals.
346
347 **Ym1 crystals activate DCs in the lymph nodes.**
348 We next studied whether innate immunity triggered by pseudo-CLCs was accompanied by the
349 induction of adaptive immunity, particularly since IL-1$\beta$, IL-33, IL-6 and TNF$\alpha$ in the lungs can
350 activate antigen presenting cells [42]. Airway DCs bridge innate and adaptive immunity and can
351 be activated by recombinant Gal10 crystals and UA crystals [34,41]. Different subsets of DCs can
352 be clearly distinguished from recruited monocytes and resident macrophages based on the
353 expression of CD26 and lack of expression of the complement C5a receptor CD88, and further
354 separated into XCR1$^+$ cDC1 and CD172 (SIRP$\alpha$)$^+$ cDC2 (see Fig. 3A for gating strategy) [30,43]. In
355 mice given Ym1 crystals in the presence of fluorescently-labeled OVA antigen (Fig. 3 B), there
356 was a clear increase in the number of total lung-draining mLN CD26$^+$CD88$^-$CD11c$^+$CD64$^-$
357 conventional DCs (cDCs), numerically mainly caused by an increase in the number of CD172$^+$
358 cDC2, compared with mice receiving PBS or soluble Ym1, although XCR1$^+$ cDC1s also clearly
359 reacted to the crystals. There was also an increase in the number of mLN CD88$^+$CD11b$^+$
360 monocytes that expressed intermediate levels of CD11c induced by crystals (Fig. 3 C). Not
361 surprisingly, the exposure to crystalline Ym1 also led to an increase in cDC1s, cDC2s and
362 monocytes taking up the co-administered fluorescent OVA antigen (Fig. 3 D). Exposure to
363 soluble Ym1 and Ym1 crystals also induced an upregulation of the costimulatory molecules
364 CD80 (data not shown) and CD86, and this effect was most pronounced with crystalline Ym1,
365 and particularly in cDCs that were also taking up fluorescent OVA (Fig. 3 E).
366
367 **Ym1 crystals boost adaptive type 2 immunity.**
368 We next asked whether crystalline or soluble Ym1 could boost adaptive cellular immunity to
369 co-administered OVA, when DCs that have taken up antigen and matured migrate to mLNs
370 (Fig. 4 A). To evaluate induction of type 2 immunity in naïve antigen-specific T cells directly,
371 cell tracer violet labeled OVA-reactive CD4$^+$ T cell receptor (TCR) MHCII-restricted transgenic
372 T cells (OT-II T cells) crossed to the huCD2-IL-4 (KN2) reporter strain were transferred into WT
373 mice, allowing us to track T cell division simultaneously with the acquisition of a Th2-polarized

374 state *in vivo* [44]. When innocuous OVA was injected i.t. together with Ym1 crystals, the
375 adoptively transferred OT-II KN2 T cells showed increased proliferation 4 days (Fig. 4 B) and 7
376 days (data not shown) later in the mLNs, an effect absent when OVA was given with soluble
377 Ym1. This led to the accumulation of higher numbers of OT-II T cells and Th2 polarizing KN2+
378 OT-II T cells in the mLNs 4 days (Fig. 4 C) and 7 days (Fig. 4 D) after the i.t. administration. After
379 7 days, divided OT-II T cells and KN2+ OT-II T cells could also be found in the lungs of mice
380 receiving OVA mixed with Ym1 crystals (Fig. 4 E). These cells lost CD62L expression while
381 expressing CD44, showing they had become effector cells (data not shown). These effects on
382 T cell activation and Th2 polarization were again not observed when OVA was injected
383 together with soluble Ym1. Early IL-4 production in OVA-reactive OT-II cells could also point
384 to differentiation of T cells into $T_{FH}$ cells that provide help for germinal center reactions.
385 However, we did not add CXCR5 or PD1 to study $T_{FH}$ development in greater detail.
386
387 We finally tested whether Ym1 crystals could also promote allergic type 2 inflammation to
388 inhaled harmless antigens, typically observed in asthmatics. WT C57BL/6 mice were sensitized
389 i.t. with OVA mixed with Ym1 crystals on days 0 and 1 and received OVA i.n. challenges on
390 days 11 to 13 (Fig. 5 A). These mice exhibited airway inflammation characterized by an influx
391 of eosinophils, B cells and T cells (Fig. 5 B), a higher production of the type 2 cytokines IL-5, IL-
392 10 and IL-13 in the supernatants of mLN restimulation cultures (Fig. 5 C) and a robust OVA-
393 specific IgG1 response, a hallmark of type 2 immunity, most likely driven by enhanced IL-4
394 production in Th2 or $T_{FH}$ cells (Fig. 5 D). These effects were not observed when OVA alone was
395 used as the immunogen or when OVA was co-administered with soluble Ym1. Thus, the
396 induction of allergic type 2 inflammation was specifically related to the crystalline state of
397 Ym1. In contrast to recombinant Gal10 crystals, which mounted high titers of Gal10-specific
398 IgG1 antibodies when used as adjuvant in the same experimental set-up [34], Ym1 crystals did
399 not elicit an antibody response directed to Ym1 (Fig. 5 E). However, when mice received
400 repetitive injections of Ym1 crystals in a different set-up via i.p. injection (Fig. 5 F), high titers
401 of Ym1-specific IgM were detected (Fig. 5 G), suggesting that Ym1 crystals can trigger an auto-
402 immune response or elicit a recall response from natural IgM antibody producing peritoneal
403 B cells.
404
405

406 **Discussion**

407 Ym1 and Ym2 are among the most strongly induced proteins in the airways of mice after
408 allergen exposure[45-49] and both proteins readily form pseudo-CLCs *in vivo.* As a result, Ym1
409 and Ym2 have become markers of type 2 inflammation. Here we show that the phase
410 transition of soluble Ym1/Ym2 to crystalline pseudo-CLC states leads to profound
411 immunostimulatory effects on innate and adaptive type 2 immunity. Sutherland and
412 colleagues have shown that vector-based overexpression of Ym1 or Ym2 in the lung increased
413 the number of neutrophils in the BAL fluid. Moreover, blocking antibodies directed against
414 Ym1/2 also suppressed neutrophilic inflammation in the lungs of asthmatic mice and
415 helminth-infected mice [50]. Whether these observed effects were due to the crystalline or
416 soluble state of Ym1/2 remains unclear from these studies. Also in the present study, we
417 lacked a proper soluble Ym1 control, since ImageStream analysis showed the soluble Ym1
418 protein to readily crystallize upon injection in the lungs. So far, several attempts to produce
419 crystallization-deficient soluble Ym1 or Ym2 muteins failed, despite the fact that this was
420 feasible for the CLC protein Gal10 [34]. Antibodies to Gal10 also dissolved pre-existing CLCs, but
421 from the published literature it is unclear if the Ym1/Ym2 antibodies used would also suppress
422 lung neutrophilia by dissolving Ym1/2 pseudo-CLC [34,50]. We also observed that Ym1 crystals
423 induced an auto-antibody response of the IgM isotype, suggesting intrinsic adjuvant activity
424 in the crystalline state of Ym1. Antibodies to Ym1/2 have been described to occur also in a
425 model of incipient neoplasia in mice overexpressing the Epstein Barr virus oncogene LMP1 in
426 the skin, leading to chronic inflammation[51]. However, it is unclear if induction of such auto-
427 antibodies to Ym1/2 would be the result of spontaneous crystallization of Ym1/2 in the skin
428 of these mice. Recognition of endogenously produced UA or cholesterol crystals by IgM has
429 been described previously [52,53], and in the case of UA, it was even proposed that IgM is
430 required to turn soluble UA into an immunostimulatory adjuvant [53]. Future studies will have
431 to establish if IgM contributes in some way to the adjuvanticity of Ym1 crystals or facilitates
432 the transition of soluble to crystalline Ym1.

433 Ym1 (*Chil3*) and Ym2 (*Chil4*) share 95% nucleotide sequence identity and 91% amino acid
434 sequence identity and we now show here that native *in vivo* grown Ym1 crystals are
435 structurally similar to native *in vivo* grown Ym2 crystals. Thus, Ym2 crystals most likely will
436 stimulate innate and adaptive immunity and act as a type 2 adjuvant, similar to Ym1 crystals,
437 although we did not formally demonstrate this experimentally.

438 Understanding the requirements for protein crystal formation during type 2 immunity,
439 studying the mechanisms whereby protein crystals stimulate type 2 immunity and having the
440 proper tools to be able to distinguish between the soluble and the crystalline state will help
441 us to better understand if targeting CLCs in human asthma and CRSwNP would be of value.
442 Since CLCs and pseudo-CLCs are almost exclusively found in eosinophilic airway inflammation
443 across many species, and share many biological effects, it appears that protein crystallization
444 is a more generalized feature of type 2 immunity. The convergent evolution of CLCs and
445 pseudo-CLCs as protein crystals in type 2 immunity strongly suggests a selective advantage of
446 these protein crystals in the enhancement of type 2-driven immune responses.

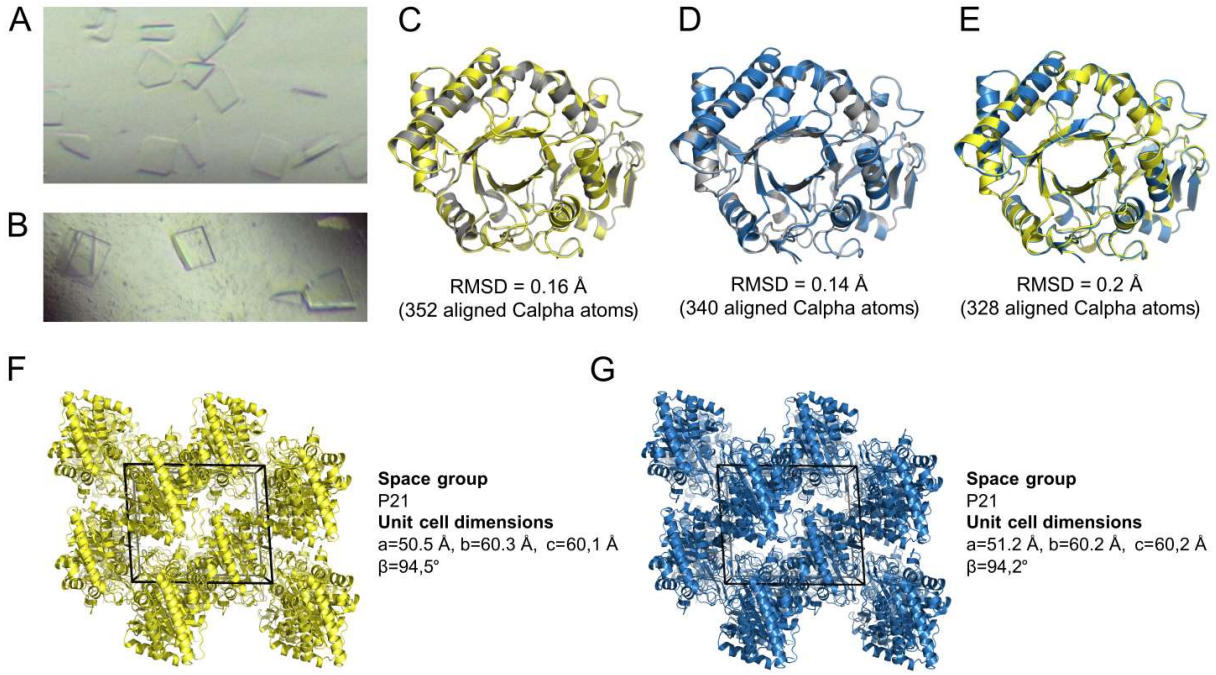


**Figure 1: Recombinant Ym1 and Ym2 crystals are structurally similar to *in vivo* Ym1 and Ym2 crystals and to each other. A, B)** Light microscopy pictures of recombinant Ym1 (A) and Ym2 (B) crystals. **C-E)** Structural superposition of the X-ray structures determined from a native *in vivo* grown Ym1 crystal isolated from the BAL fluid of $me^{v}/me^{v}$ mice (C+E) (yellow), a native *in vivo* grown Ym2 crystal isolated from the BAL fluid of a C57BL/6J-Tg(CAG-Gal10)Bla mouse (D+E) (blue) and a recombinant Ym1 (C) and Ym2 (D) crystal (grey). The low root-mean-square deviations (RMSDs) establish structural similarity. **F, G)** Crystal packing of *ex vivo* Ym1 (F) and Ym2 (G) crystals revealing their crystallographic equivalence.

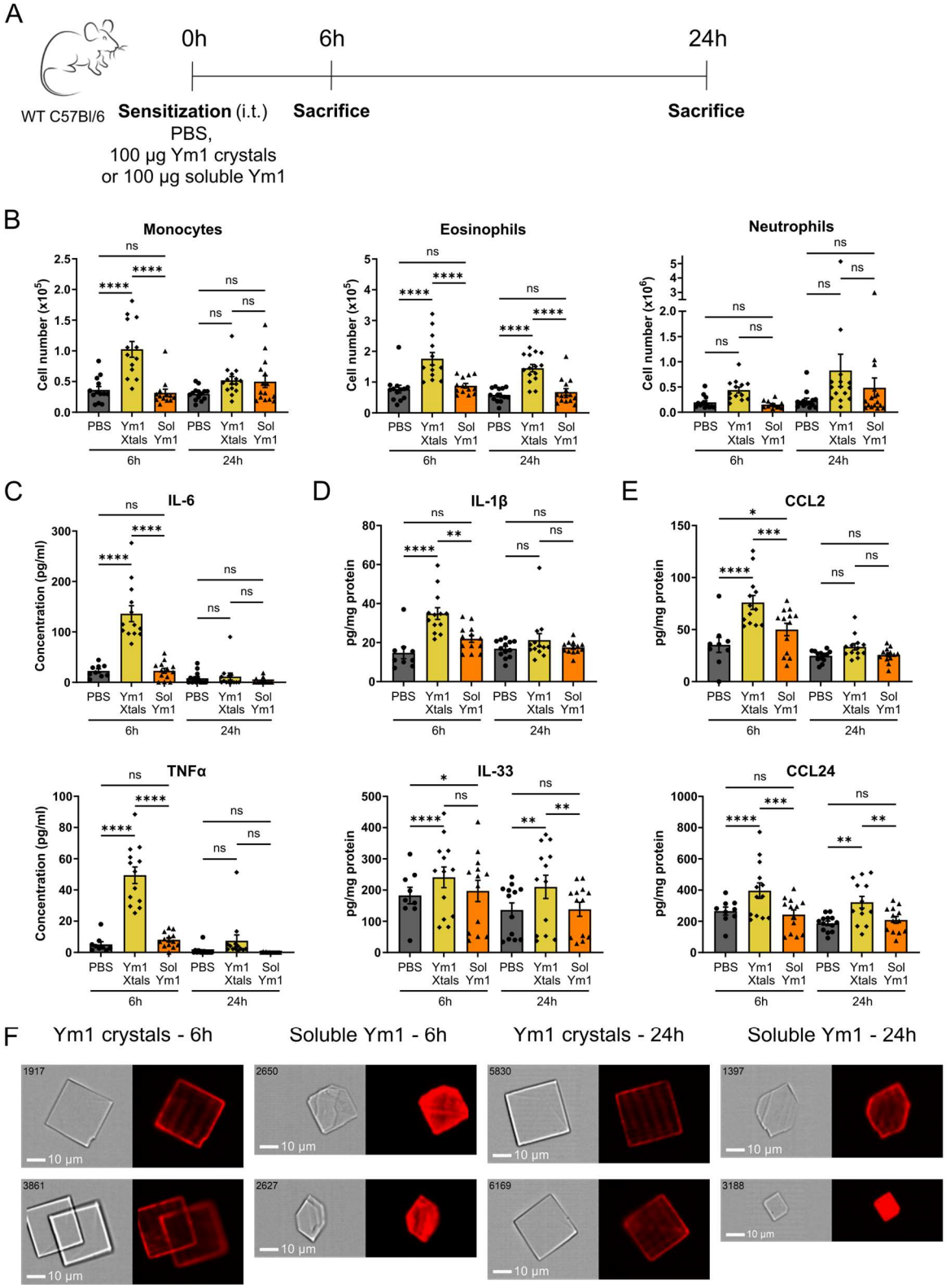


**Figure 2: Ym1 crystals activate innate immunity. A)** Scheme representing the innate immune response experiment. **B)** Flow cytometric analysis of the immune cell influx in the lungs of PBS, Ym1 crystal and soluble Ym1 treated mice measured 6 and 24 hours after i.t. injection. Data are pooled from 2 (for 6h time point) or 3 (for 24h time point) independent experiments with n = 13, 13, 13, 14, 15 and 15, respectively. **C)** Concentration of IL-6 and TNFα in the BAL fluid measured by ELISA. **D, E)** Concentration of IL-1β, IL-33 (D), CCL2 and CCL24 (E) per milligram of protein of dispersed lung tissue measured by ELISA. Data are pooled from 2 independent experiments with n = 13 per group. Data are shown as

466 mean ± SEM. ns P ≥ 0.05; *P < 0.05; **P<0,01; ***P <0.001; ****P < 0.0001. **E)** ImageStream pictures
467 of the BAL fluid of Ym1 crystal and soluble Ym1 treated mice 6 and 24 hours after i.t. injection. Samples
468 were stained with an antibody recognizing Ym1/2 (red).
469

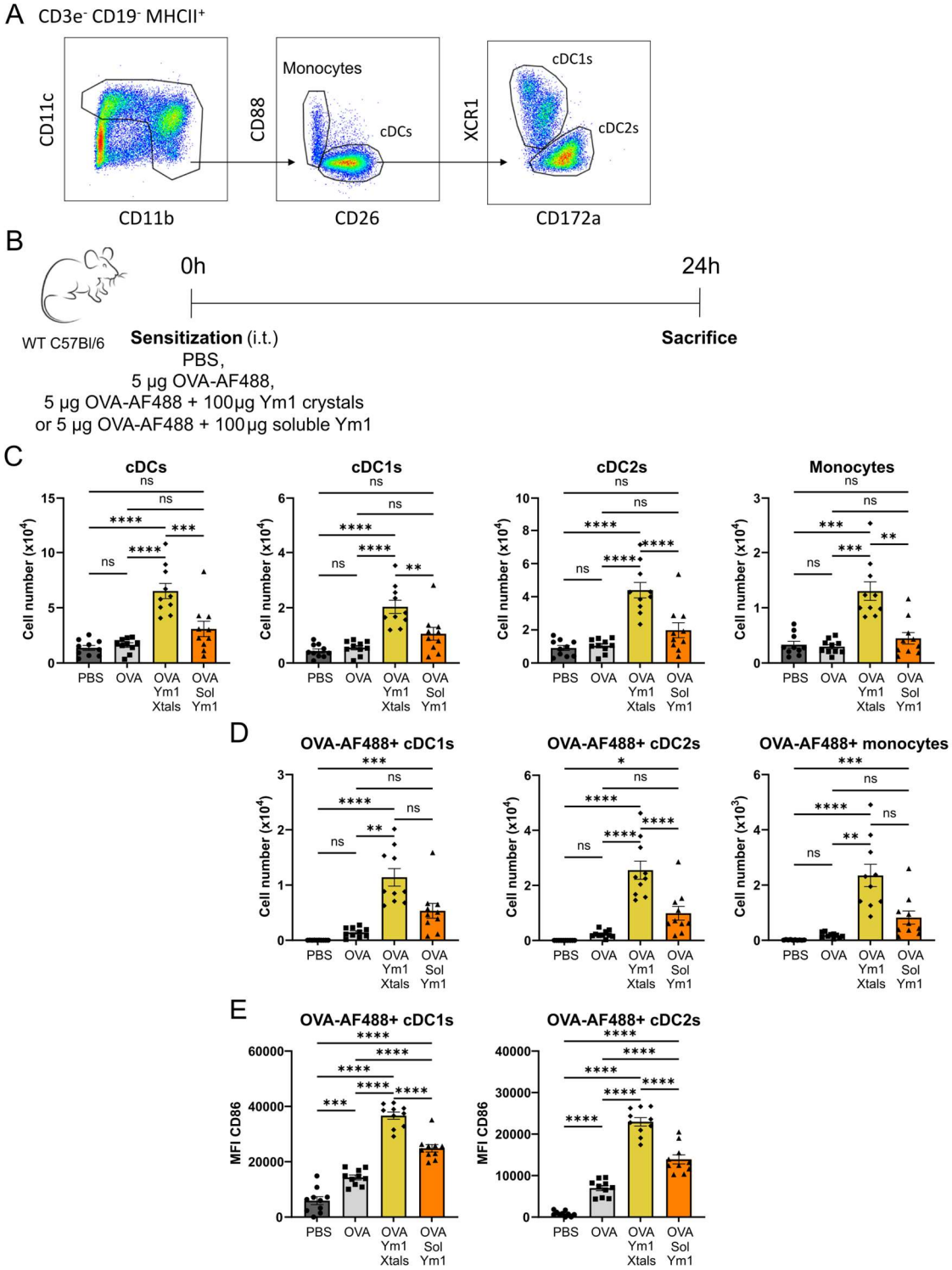


**Figure 3: Ym1 crystals activate DCs in the lymph nodes. A)** Gating strategy to distinguish different subsets of DCs and recruited monocytes. **B)** Scheme representing the DC activation experiment. **C, D)** Flow cytometric analysis of the DC and monocyte influx in the mLNs of PBS, OVA-AF488 alone, OVA-AF488 plus Ym1 crystals and OVA-AF488 plus soluble Ym1 treated mice measured 24 hours after i.t. injection. **E)** Median Fluorescence Intensity (MFI) of activation marker CD86 on OVA-AF488+ cDC1s and cDC2s of PBS, OVA-AF488 alone, OVA-AF488 plus Ym1 crystals and OVA-AF488 plus soluble Ym1 treated mice measured 24 hours after i.t. injection. Data are pooled from 2 independent experiments with n = 10 mice per group. Data are shown as mean ± SEM. ns P ≥ 0.05; *P < 0.05; **P<0,01; ***P <0.001; ****P < 0.0001.

480

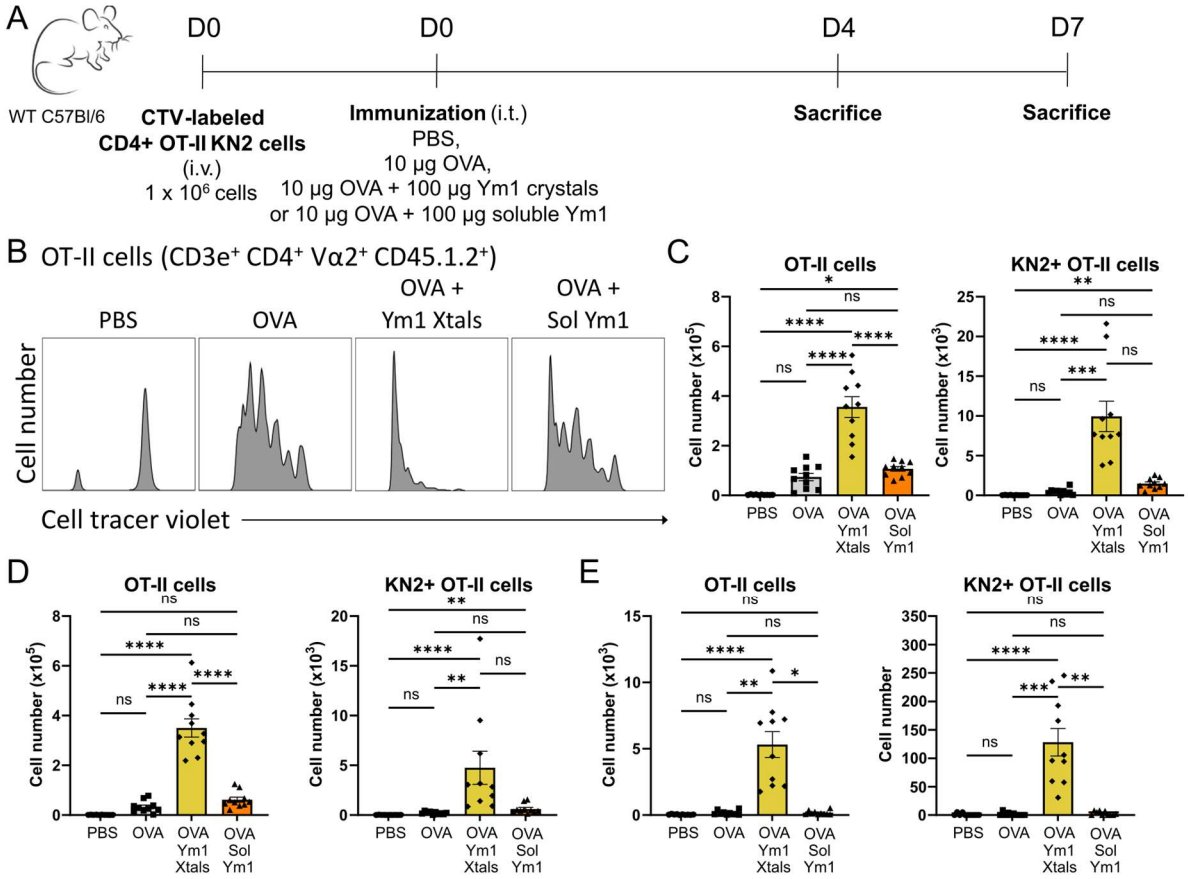


481

482 **Figure 4: Ym1 crystals boost adaptive cellular immunity. A)** Scheme representing the used adoptive
483 transfer model. **B-E)** Proliferation and KN2 expression of OT-II T cells in the mLNs and lungs 4 and 7
484 days after i.t. administration of PBS, OVA alone, OVA plus Ym1 crystals or OVA plus soluble Ym1. (B)
485 Representative histograms of the division profile of the adoptively transferred OT-II T cells ($CD3e^+$
486 $CD4^+$ $V\alpha2^+$ $CD45.1.2^+$) in the mLNs on day 4. (C, D) The numbers of OT-II T cells and KN2+ OT-II T cells
487 in the mLNs on day 4 (C) and day 7 (D). (E) The numbers of OT-II T cells and KN2+ OT-II T cells in the
488 lungs on day 7. Data are pooled from 2 independent experiments with n = 10 mice per group. Data
489 are shown as mean ± SEM. ns $P \geq 0.05$; *$P < 0.05$; **P<0,01; ***P <0.001; ****$P < 0.0001$.

490

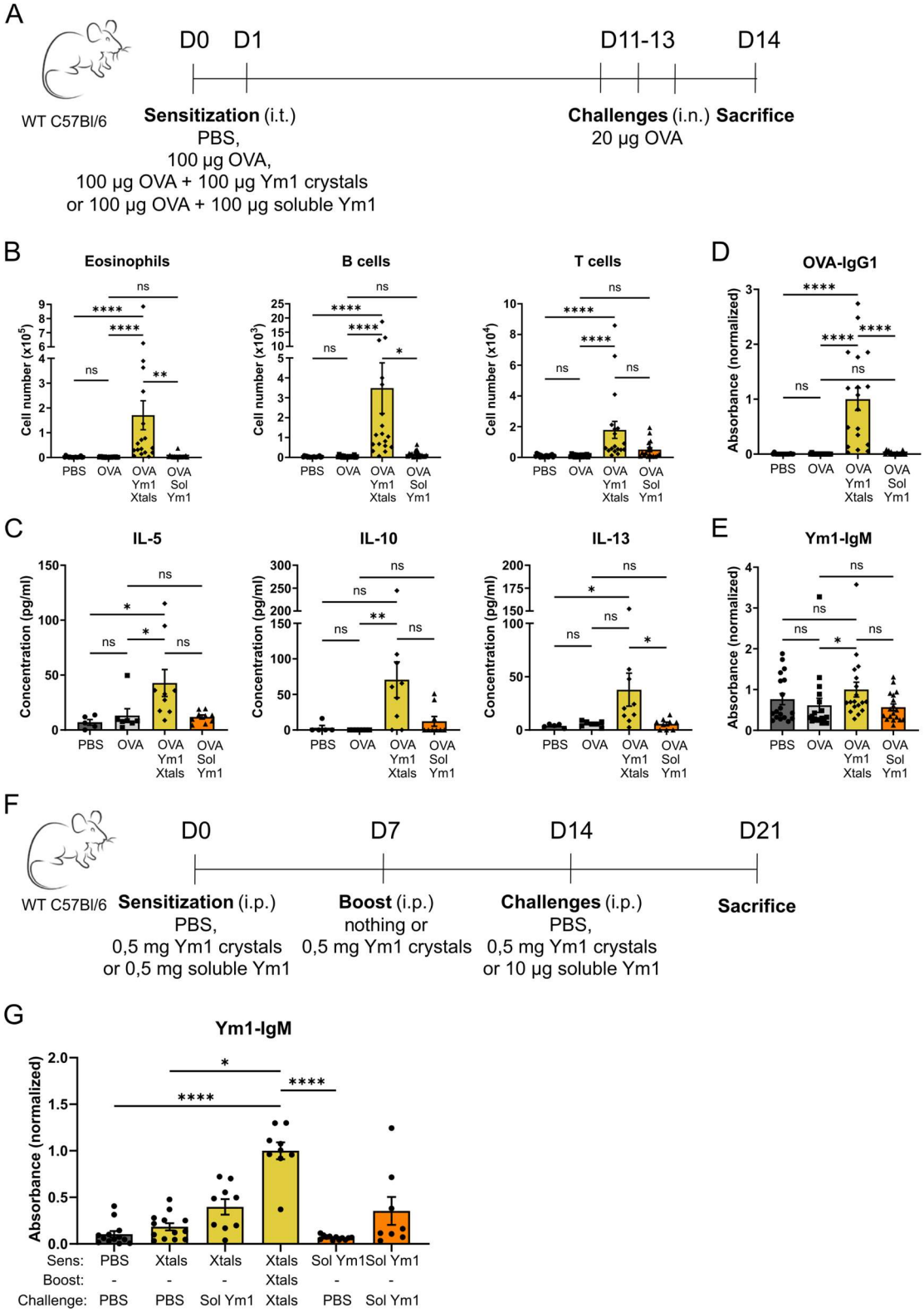


**Figure 5: Ym1 crystals can act as type 2 adjuvant in OVA-induced asthma model and activate adaptive humoral immunity. A)** Scheme representing the used OVA-induced asthma model. **B)** Flow cytometric analysis of the immune cell influx in the BAL fluid of mice sensitized i.t. with PBS, OVA alone, OVA plus Ym1 crystals or OVA plus soluble Ym1 and challenged i.n. with OVA. Data are pooled from 2 independent experiments with n = 18 per group. **C)** Levels of IL-5, IL-10 and IL-13 in the supernatant of mLN cells after restimulation with OVA for 20 hours. Data are from 1 experiment with n = 5, 7, 9 and 9, respectively. **D)** Serum OVA-specific IgG1 antibodies were measured by ELISA. **E)** Serum Ym1-specific

IgM antibodies were measured by ELISA. Data are pooled from 2 independent experiments with n = 18 per group. **F)** Scheme representing the adaptive humoral immune response experiment. **G)** Serum Ym1-specific IgM antibodies were measured by ELISA. Data are pooled from 3 independent experiments with n = 13, 13, 9, 9, 12 and 8, respectively. Data are shown as mean ± SEM. ns $P \geq 0.05$; *$P < 0.05$; **P<0,01; ****$P < 0.0001$. If pairwise comparison is not shown, the result is not significant.

## References


1. Charcot, J. & Vulpian, A. Note sur des cristaux particuliers trouvés dans le sang et dans certains viscèresd'un sujet leucémique, et sur d'autres faits necroscopiques observés sur le même sujet. *Gaz. Hebd. de Méd et Chirurgie*, 755-758 (1860).
2. von Leyden, E. Zur Kenntniss des bronchial asthma. *(Virchov) Arch. Pathol. Anat.* **54**, 324-344. (1872).
3. Aegerter, H.*, et al.* Charcot-Leyden crystals and other protein crystals driving type 2 immunity and allergy. *Curr Opin Immunol* **72**, 72-78 (2021).
4. Doye, J.P., Louis, A.A. & Vendruscolo, M. Inhibition of protein crystallization by evolutionary negative design. *Phys Biol* **1**, P9-13 (2004).
5. Schonherr, R., Rudolph, J.M. & Redecke, L. Protein crystallization in living cells. *Biol Chem* **399**, 751-772 (2018).
6. Guo, L., Johnson, R.S. & Schuh, J.C. Biochemical characterization of endogenously formed eosinophilic crystals in the lungs of mice. *J Biol Chem* **275**, 8032-8037 (2000).
7. Hoenerhoff, M.J., Starost, M.F. & Ward, J.M. Eosinophilic crystalline pneumonia as a major cause of death in 129S4/SvJae mice. *Vet Pathol* **43**, 682-688 (2006).
8. Takamoto, M.*, et al.* Eosinophilia, parasite burden and lung damage in Toxocara canis infection in C57Bl/6 mice genetically deficient in IL-5. *Immunology* **90**, 511-517 (1997).
9. Shultz, L.D., Coman, D.R., Bailey, C.L., Beamer, W.G. & Sidman, C.L. "Viable motheaten," a new allele at the motheaten locus. I. Pathology. *Am J Pathol* **116**, 179-192 (1984).
10. Harbord, M.*, et al.* Ym1 is a neutrophil granule protein that crystallizes in p47phox-deficient mice. *J Biol Chem* **277**, 5468-5475 (2002).
11. Liu, Q.*, et al.* p47phox deficiency induces macrophage dysfunction resulting in progressive crystalline macrophage pneumonia. *Am J Pathol* **174**, 153-163 (2009).
12. Waern, I.*, et al.* Accumulation of Ym1 and formation of intracellular crystalline bodies in alveolar macrophages lacking heparanase. *Mol Immunol* **47**, 1467-1475 (2010).
13. Poczobutt, J.M.*, et al.* Altered Macrophage Function Associated with Crystalline Lung Inflammation in Acid Sphingomyelinase Deficiency. *Am J Respir Cell Mol Biol* **64**, 629-640 (2021).
14. Fallon, P.G., Emson, C.L., Smith, P. & McKenzie, A.N. IL-13 overexpression predisposes to anaphylaxis following antigen sensitization. *J. Immunol.* **166**, 2712-2716. (2001).
15. Rehm, S., Wcislo, A. & Deerberg, F. Non-neoplastic lesions of female virgin Han:NMRI mice, incidence and influence of food restriction throughout life span. II: Respiratory tract. *Lab Anim* **19**, 224-235 (1985).
16. Green, E. On the occurrence of crystalline material in the lungs of normal and cancerous Swiss mice. *Cancer Res* **2**, 210-217 (1942).
17. Murray, A.B. & Luz, A. Acidophilic macrophage pneumonia in laboratory mice. *Vet Pathol* **27**, 274-281 (1990).
18. Yang, Y.H. & Campbell, J.S. Crystalline Excrements in Bronchitis and Cholecystitis of Mice. *Am J Pathol* **45**, 337-345 (1964).
19. Feldmesser, M., Kress, Y. & Casadevall, A. Intracellular crystal formation as a mechanism of cytotoxicity in murine pulmonary Cryptococcus neoformans infection. *Infect Immun* **69**, 2723-2727 (2001).
20. Baldan, A., Gomes, A.V., Ping, P. & Edwards, P.A. Loss of ABCG1 results in chronic pulmonary inflammation. *J Immunol* **180**, 3560-3568 (2008).
21. Huffnagle, G.B., Boyd, M.B., Street, N.E. & Lipscomb, M.F. IL-5 is required for eosinophil recruitment, crystal deposition, and mononuclear cell recruitment during a pulmonary Cryptococcus neoformans infection in genetically susceptible mice (C57BL/6). *J. Immunol.* **160**, 2393-2400 (1998).
22. Mall, M.A.*, et al.* Development of chronic bronchitis and emphysema in beta-epithelial Na+ channel-overexpressing mice. *Am J Respir Crit Care Med* **177**, 730-742 (2008).

556 23. Roediger, B.*, et al.* IL-2 is a critical regulator of group 2 innate lymphoid cell function during
557 pulmonary inflammation. *J Allergy Clin Immunol* **136**, 1653-1663 e1657 (2015).
558 24. Henderson, W.R., Jr.*, et al.* A role for cysteinyl leukotrienes in airway remodeling in a mouse
559 asthma model. *Am J Respir Crit Care Med* **165**, 108-116 (2002).
560 25. Zhu, Z.*, et al.* Pulmonary expression of interleukin-13 causes inflammation, mucus
561 hypersecretion, subepithelial fibrosis, physiologic abnormalities, and eotaxin production. *J*
562 *Clin Invest* **103**, 779-788 (1999).
563 26. Leonidas, D.D.*, et al.* Crystal structure of human Charcot-Leyden crystal protein, an
564 eosinophil lysophospholipase, identifies it as a new member of the carbohydrate-binding
565 family of galectins. *Structure* **3**, 1379-1393 (1995).
566 27. Swaminathan, G.J., Leonidas, D.D., Savage, M.P., Ackerman, S.J. & Acharya, K.R. Selective
567 recognition of mannose by the human eosinophil Charcot-Leyden crystal protein (galectin-
568 10): a crystallographic study at 1.8 A resolution. *Biochemistry* **38**, 13837-13843 (1999).
569 28. Raes, G.*, et al.* Differential expression of FIZZ1 and Ym1 in alternatively versus classically
570 activated macrophages. *J Leukoc Biol* **71**, 597-602 (2002).
571 29. Ikeda, N.*, et al.* Emergence of immunoregulatory Ym1(+)Ly6C(hi) monocytes during recovery
572 phase of tissue injury. *Sci Immunol* **3**(2018).
573 30. Aegerter, H., Lambrecht, B.N. & Jakubzick, C.V. Biology of lung macrophages in health and
574 disease. *Immunity* **55**, 1564-1580 (2022).
575 31. Ward, J.M.*, et al.* Hyalinosis and Ym1/Ym2 gene expression in the stomach and respiratory
576 tract of 129S4/SvJae and wild-type and CYP1A2-null B6, 129 mice. *Am J Pathol* **158**, 323-332
577 (2001).
578 32. Parkinson, J.E., Pearson, S., Ruckerl, D., Allen, J.E. & Sutherland, T.E. The magnitude of airway
579 remodeling is not altered by distinct allergic inflammatory responses in BALB/c versus
580 C57BL/6 mice but matrix composition differs. *Immunol Cell Biol* **99**, 640-655 (2021).
581 33. Van Dyken, S.J. & Locksley, R.M. Chitins and chitinase activity in airway diseases. *J Allergy Clin*
582 *Immunol* **142**, 364-369 (2018).
583 34. Persson, E.K.*, et al.* Protein crystallization promotes type 2 immunity and is reversible by
584 antibody treatment. *Science* **364**, 10.1126/science.aaw4295 (2019).
585 35. Kabsch, W. Integration, scaling, space-group assignment and post-refinement. *Acta*
586 *Crystallogr D Biol Crystallogr* **66**, 133-144 (2010).
587 36. Winn, M.D.*, et al.* Overview of the CCP4 suite and current developments. *Acta Crystallogr D*
588 *Biol Crystallogr* **67**, 235-242 (2011).
589 37. McCoy, A.J.*, et al.* Phaser crystallographic software. *J Appl Crystallogr* **40**, 658-674 (2007).
590 38. Emsley, P., Lohkamp, B., Scott, W.G. & Cowtan, K. Features and development of Coot. *Acta*
591 *Crystallographica Section D: Biological Crystallography* **66**, 486-501 (2010).
592 39. Bricogne G., B.E., Brandl M., Flensburg C., Keller P., Paciorek W., & Roversi P, S.A., Smart O.S.,
593 Vonrhein C., Womack T.O. . BUSTER version 2.10.3 *Cambridge, United Kingdom: Global*
594 *Phasing Ltd.* (2017).
595 40. Joosten, R.P., Long, F., Murshudov, G.N. & Perrakis, A. The PDB_REDO server for
596 macromolecular structure model optimization. *IUCrJ* **1**, 213-220 (2014).
597 41. Kool, M.*, et al.* An unexpected role for uric acid as an inducer of T helper 2 cell immunity to
598 inhaled antigens and inflammatory mediator of allergic asthma. *Immunity* **34**, 527-540
599 (2011).
600 42. Lambrecht, B.N. & Hammad, H. Lung dendritic cells in respiratory viral infection and asthma:
601 from protection to immunopathology. *Annu Rev Immunol* **30**, 243-270 (2012).
602 43. Rawat, K.*, et al.* CCL5-producing migratory dendritic cells guide CCR5+ monocytes into the
603 draining lymph nodes. *J Exp Med* **220**(2023).
604 44. Mohrs, M., Shinkai, K., Mohrs, K. & Locksley, R. Analysis of type 2 immunity in vivo with a
605 bicistronic reporter. *Immunity* **15**, 303-311 (2001).
606 45. Jeong, H.*, et al.* Proteomic analysis of differently expressed proteins in a mouse model for
607 allergic asthma. *J Korean Med Sci* **20**, 579-585 (2005).

46. Zhao, J., Zhu, H., Wong, C.H., Leung, K.Y. & Wong, W.S. Increased lungkine and chitinase levels in allergic airway inflammation: a proteomics approach. *Proteomics* **5**, 2799-2807 (2005).
47. Zhao, J., Yeong, L.H. & Wong, W.S. Dexamethasone alters bronchoalveolar lavage fluid proteome in a mouse asthma model. *Int Arch Allergy Immunol* **142**, 219-229 (2007).
48. Wong, W.S., Zhu, H. & Liao, W. Cysteinyl leukotriene receptor antagonist MK-571 alters bronchoalveolar lavage fluid proteome in a mouse asthma model. *Eur J Pharmacol* **575**, 134-141 (2007).
49. Wong, W.S. & Zhao, J. Proteome analysis of chronically inflamed lungs in a mouse chronic asthma model. *Int Arch Allergy Immunol* **147**, 179-189 (2008).
50. Sutherland, T.E.*, et al.* Chitinase-like proteins promote IL-17-mediated neutrophilia in a tradeoff between nematode killing and host damage. *Nat Immunol* **15**, 1116-1125 (2014).
51. Qureshi, A.M., Hannigan, A., Campbell, D., Nixon, C. & Wilson, J.B. Chitinase-like proteins are autoantigens in a model of inflammation-promoted incipient neoplasia. *Genes Cancer* **2**, 74-87 (2011).
52. Pilely, K.*, et al.* Cholesterol Crystals Activate the Lectin Complement Pathway via Ficolin-2 and Mannose-Binding Lectin: Implications for the Progression of Atherosclerosis. *J Immunol* **196**, 5064-5074 (2016).
53. Kanevets, U., Sharma, K., Dresser, K. & Shi, Y. A role of IgM antibodies in monosodium urate crystal formation and associated adjuvanticity. *J Immunol* **182**, 1912-1918 (2009).

630 **Table S1. Crystallographic data and refinement statistics[§,*]**

| Protein complex | Recombinant Ym1 | *Ex vivo* Ym1 | Recombinant Ym2 | *Ex vivo* Ym2 |
|---|---|---|---|---|
| **Data collection** | | | | |
| X-ray source (beamline) | SOLEIL (Proxima 1) | PETRA III (P14) | PETRA III (P14) | SLS (PXI) |
| Wavelength (λ) | 0.97857 | 0.9763 | 0.9763 | 1.0000089224 |
| Space group | *P21* | *P21* | *P21* | *P21* |
| Cell dimensions | | | | |
| *a*, *b*, *c* (Å) | 50.33, 60.01, 60.12 | 50.52, 60.25, 60.12 | 51.09, 59.90, 59.88 | 51.16, 60.21, 60.17 |
| α, β, γ (°) | 90.00, 94.66, 90.00 | 90.00, 94.48, 90.00 | 90.00, 94.14, 90.00 | 90.00, 94.24, 90.00 |
| Resolution (Å) | 50.00-1.79 (1.90-1.79) | 59.93-1.42 (1.50-1.42) | 59.90-1.17 (1.24-1.17) | 42.50-1.70 (1.81-1.70) |
| $R_{meas}$ (%) | 24.7 (112.1) | 12.2 (138.2) | 8.0 (35.8) | 17.7 (136.4) |
| $< I/\sigma >$ | 5.28 (1.54) | 8.99 (1.19) | 15.12 (4.74) | 6.59 (0.96) |
| CC ½ (%) | 97.9 (56.6) | 99.7 (39.5) | 99.9 (92.5) | 99.2 (35.8) |
| Completeness (%) | 99.2 (96.0) | 98.1 (97.3) | 98.4 (95.9) | 97.7 (97.3) |
| Redundancy | 4.1 (3.9) | 3.3 (3.3) | 6.8 (6.1) | 3.5 (3.4) |
| ISa score | 8.04 | 26.18 | 27.31 | 24.20 |
| Wilson B ($Å^2$) | 20.318 | 20.936 | 12.048 | 24.584 |
| **Refinement** | | | | |
| Resolution (Å) | 42.40-1.79 | 26.91-1.42 | 37.45-1.17 | 16.78-1.71 |
| No. reflections | 33 407 | 66 944 | 119 181 | 39 026 |
| $R_{work}$ / $R_{free}$ (%) | 17.29 / 19.86 | 18.10 / 20.52 | 15.75 / 16.83 | 17.71 / 20.48 |
| No. non-H atoms | | | | |
| Protein | 2 957 | 2 957 | 2 976 | 2 970 |
| Ligand/ion | 10 | 4 | 24 | 6 |
| Water | 215 | 163 | 584 | 239 |
| *B*-factors ($Å^2$) | | | | |
| Protein | 12.09 | 15.58 | 10.28 | 18.50 |
| Ligand/ion | 21.52 | 30.73 | 16.20 | 30.69 |
| Water | 21.74 | 22.78 | 27.02 | 27.93 |
| R.m.s. deviations | | | | |
| Bond lengths (Å) | 0.008 | 0.010 | 0.010 | 0.010 |
| Bond angles (°) | 0.91 | 0.98 | 1.07 | 0.97 |

631 [§]Each dataset was collected from a single crystal. *Values in parentheses are for highest-resolution shell.
632